

Isomeric excitation of ^{229}Th via scanning tunneling microscope

Xue Zhang, Tao Li, Xu Wang,* and Hui Dong†

Graduate School of China Academy of Engineering Physics,
No. 10 Xibeiwang East Road, Haidian District, Beijing, 100193, China

The low energy of the isomeric state of the radionuclide thorium-229 (^{229}Th) makes it highly promising for applications in fundamental physics, precision metrology, and quantum technologies. However, directly accessing the isomeric state from its ground state remains a challenge. We propose here a tabletop approach utilizing the scanning tunneling microscope (STM) technique to induce excitation of a single ^{229}Th nucleus. With achievable parameters, the isomeric excitation rate is advantageous over existing methods, allowing the excitation and control of ^{229}Th on the single-nucleus level. It offers the unique potential of exciting and detecting subsequent γ decay from a single nucleus, providing a new direction for future experimental investigation of the ^{229}Th isomeric state.

Introduction.— ^{229}Th recently garnered significant attention due to its low-lying isomeric state [1, 2], which is only 8.3 eV above the nuclear ground state [3, 4]. It is an appealing candidate for various applications in constructing nuclear optical clocks [5–8], detecting temporal variations of fundamental constants [9–11], measuring gravitational shifts [12, 13], etc. The isomeric state can be obtained from nuclear decay reactions [4, 14, 15]. Nevertheless, to allow control and to facilitate the applications, extensive research efforts have been made to explore active nuclear-excitation approaches, using vacuum ultraviolet light sources [16–18], high-energy synchrotron radiations [19, 20], laser pulses [21–26], electrons [27, 28], muons [29, 30], etc. Currently, experimental demonstrations are only reported with high-energy synchrotron radiations [20] and laser-generated plasmas [22]. More manipulable experimental approaches are still desirable.

In this Letter, we propose a completely new experimental setup using the tabletop scanning tunneling microscopy (STM) to excite the ^{229}Th atomic nucleus to its isomeric state ^{229m}Th . STM is a powerful imaging technique used in nanotechnology and surface science [31, 32]. It relies on the principle of quantum tunneling, where a sharp metal tip scans the surface of a sample at atomic scales, detecting the flow of electrons between the tip and the surface. By mapping the electron tunneling current, STM produces high-resolution images that reveal the topography and electronic properties of materials at the atomic level. With the high spatial control of the tip, a single ^{229}Th atom can be located and controlled, as illustrated in Fig. 1. A metal tip with radius of curvature R_t is positioned above the substrate plane with distance d . Both the tip and substrate are typically made of a noble metal, e.g. silver (Ag) [33, 34]. The ^{229}Th atoms are assumed to be doped in a wide-bandgap crystal, such as CaF_2 , to suppress the internal conversion process [35]. After applying a bias voltage V_b , electrons will tunnel through the vacuum between the tip and the substrate and excite the ^{229}Th nucleus from the ground state to the isomeric state.

The current approach offers advantages on precise manipulation, isomeric-excitation efficiency, and photon-detection

efficiency. Firstly, the STM allows the precise focus of electronic current on the level nA to an area of nm scale [36], resulting in an electron flux of about $10^{10} \text{ nm}^{-2}\text{s}^{-1}$. In contrast, beam electron sources have current intensities on mA level and cm-scale area [37], yielding an electron flux of $10^2 \text{ nm}^{-2}\text{s}^{-1}$. This key difference allows (a) excitation and control of a located single ^{229}Th nucleus, and (b) much higher single-nucleus excitation rate. With currently available STM parameters (e.g. tip radius 0.5 nm, tip-substrate distance 0.5 nm, and bias voltage -11 V), the isomeric excitation rate can reach 10^{-5}s^{-1} . Further technological refinement may increase it to the level of 10^{-2}s^{-1} , opening enormous potential in single-nucleus excitation and control. Secondly, the current tabletop setup enables the application of the experimental technique of the highly efficient luminescence detection with the detection solid angle about 3 sr [38, 39], which is much greater than the solid angle of about 0.1 sr in the synchrotron radiation excitation experiment [20]. Efficient photon collection allows the detection of the weak photon signals from the radiative decay of ^{229m}Th . These advantages make the current method highly promising for achieving excitation, control, and detection of ^{229}Th especially on the single-nucleus level, which is not achievable with other methods.

Theory of Isomeric Excitation using STM.— In this part we develop a quantum theory of isomeric excitation particularly for the STM setup. The total Hamiltonian of the system is $H = H_{el} + H_n + H_{int}$, where $H_{el}(H_n)$ represents the Hamiltonian of the tunneling electron (the ^{229}Th nucleus) and H_{int} is the interaction between them. The Hamiltonian of the tunneling electron is $H_{el} = -\nabla^2/2m_e + V(\mathbf{r})$, where $V(\mathbf{r})$ is the potential felt by the tunneling electron at the position \mathbf{r} [40, 41]. The wave functions are found for different regions as [40–43]

$$\begin{aligned} H_{el,t}|\phi_k\rangle &\simeq \tilde{\xi}_k|\phi_k\rangle, \\ H_{el,s}|\varphi_n\rangle &\simeq \tilde{E}_n|\varphi_n\rangle, \end{aligned} \quad (1)$$

where $H_{el,t}(H_{el,s})$ is the Hamiltonian of the free tip (substrate) obtained by neglecting the potential in the substrate (tip) region. $|\phi_k\rangle(|\varphi_n\rangle)$ is the eigenstate of free tip (substrate) with $\tilde{\xi}_k \equiv \xi_k + eV_b$ ($\tilde{E}_n \equiv E_n$), where $\xi_k(E_n)$ is the eigenenergy with zero bias voltage. Here we neglect the change of the wave function of the tip induced by the applied voltage [44]. The detailed forms of these wave functions are presented in

* xwang@gceaep.ac.cn

† hdong@gceaep.ac.cn

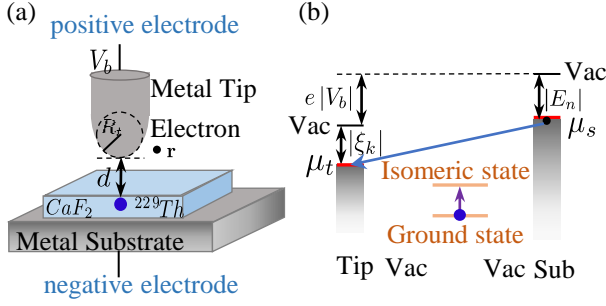


Figure 1. Schematic illustration of STM with a single ^{229}Th atom located in CaF_2 . The ^{229}Th atom is doped in a CaF_2 crystal to suppress internal conversion. The STM tip apex is modeled as a sphere with radius R_t . The position of the ^{229}Th atom (blue dot), just below the center of the tip, is set as the origin of the coordinate system, and d is the distance between the tip and substrate. \mathbf{r} stands for the position of the tunneling electron (black dot), and V_b is the bias voltage applied to the tip and substrate. (b) The energy level diagram at negative bias voltage. The black lines denote the vacuum level for two electrodes, and the red lines represent the initial and final electronic states. $\mu_t \equiv \mu_0 + eV_b$ and $\mu_s \equiv \mu_0$ are the Fermi energies of the tip and the substrate at the bias voltage V_b , where μ_0 is the Fermi energy of the tip and the substrate at zero bias.

the Supplementary Materials (SM).

The Hamiltonian of the ^{229}Th atomic nucleus is simplified as a two-level system $H_n = \epsilon_g |g\rangle \langle g| + \epsilon_e |e\rangle \langle e|$, where $|g\rangle(|e\rangle)$ is its ground (isomeric excited) state with energy $\epsilon_g(\epsilon_e)$. We assume that the energy gap is $\Delta_{eg} \equiv \epsilon_e - \epsilon_g = 8.338$ eV [4]. The interaction between the electron and nucleus is given by [45]

$$H_{int} = -\frac{1}{c} \int \mathbf{J}(\mathbf{R}) \cdot \mathbf{A}(\mathbf{R}) d\mathbf{R}, \quad (2)$$

where $\mathbf{J}(\mathbf{R})$ is the nucleus current operator at position \mathbf{R} . $\mathbf{A}(\mathbf{R})$ is the electromagnetic vector potential generated by the tunneling electron with current $\mathbf{j}(\mathbf{r})$,

$$\mathbf{A}(\mathbf{R}) = \frac{1}{c} \int \frac{e^{ik|\mathbf{r}-\mathbf{R}|}}{|\mathbf{r}-\mathbf{R}|} \cdot \mathbf{j}(\mathbf{r}) d\mathbf{r}, \quad (3)$$

where $k\hbar c = (\tilde{E}_n - \tilde{\xi}_k)$ corresponds to the energy loss of the electron. The electron current is obtained as $\mathbf{j}_{fi}(\mathbf{r}) = -e\hbar(\psi_f \nabla \psi_i^* - \psi_i^* \nabla \psi_f)/2m_e$ [32, 42]. And $\psi_i(\psi_f)$ denotes the wave function of the initial (final) state of the electron. For negative bias $V_b < 0$, the electron flies from the substrate to the tip, i.e. $\psi_i = \varphi_n(\mathbf{r})$ and $\psi_f = \phi_k(\mathbf{r})$.

From Fermi's golden rule, the transition probability per unit time from an initial state $|i\rangle$ to a final state $|f\rangle$ is written as

$$P_{fi} = \frac{2\pi}{\hbar} |\langle f | H_{int} | i \rangle|^2 \delta(\mathcal{E}_i - \mathcal{E}_f), \quad (4)$$

where for the current system $|i\rangle \equiv |J_i M_i\rangle \otimes |\varphi_n\rangle$ and $|f\rangle \equiv |J_f M_f\rangle \otimes |\phi_k\rangle$ are the product states of the nucleus and the electron. Here J_i (J_f) and M_i (M_f) are the angular momentum and magnetic quantum numbers of the nuclear ground

(isomeric) state, respectively. The initial and final energies are $\mathcal{E}_i = \epsilon_g + \tilde{E}_n$ and $\mathcal{E}_f = \epsilon_e + \tilde{\xi}_k$.

Here we use multipole expansion [45]

$$\frac{e^{ik|\mathbf{r}-\mathbf{R}|}}{|\mathbf{r}-\mathbf{R}|} = 4\pi ik \sum_{\mathcal{T}, l, m} \mathcal{A}_{lm}^{\mathcal{T}}(kR) \mathcal{B}_{lm}^{\mathcal{T}}(kr). \quad (5)$$

The transition type \mathcal{T} can be either E (electric) or M (magnetic). And $\mathcal{A}_{lm}^{\mathcal{T}}(kR)$ is the multipole vector potential, $\mathcal{A}_{lm}^M(kR) = 1/\sqrt{l(l+1)} \mathbf{L} j_l(kR) Y_{lm}(\hat{\mathbf{R}})$ and $\mathcal{A}_{lm}^E(kR) = -i/(k\sqrt{l(l+1)}) \nabla \times \mathbf{L} j_l(kR) Y_{lm}(\hat{\mathbf{R}})$. Here $Y_{lm}(\hat{\mathbf{R}})$ are spherical harmonics. The potential $\mathcal{B}_{lm}^{\mathcal{T}}(kr)$ can be obtained from $\mathcal{A}_{lm}^{\mathcal{T}}(kR)$ by replacing the Bessel function $j_l(kR)$ with the Hankel function of the first kind $h_l^{(1)}(kr)$. Then the transition matrix element $\langle f | H_{int} | i \rangle$ turns into [27, 28, 45]

$$\begin{aligned} \langle f | H_{int} | i \rangle &= \sum_{\mathcal{T}} \langle f | H_{int}^{\mathcal{T}} | i \rangle \\ &= -\frac{4\pi ik}{c^2} \sum_{\mathcal{T}, l, m} \int \mathbf{J}_{fi}(\mathbf{R}) \cdot \mathcal{A}_{lm}^{\mathcal{T}}(kR) d\mathbf{R} \\ &\quad \times \int \mathbf{j}_{fi}(\mathbf{r}) \cdot \mathcal{B}_{lm}^{\mathcal{T}}(kr) d\mathbf{r}. \end{aligned} \quad (6)$$

The first integral in the above equation associated to the nuclear transition current $\mathbf{J}_{fi}(\mathbf{R})$ is derived with the following form [27]

$$\begin{aligned} \int \mathbf{J}_{fi}(\mathbf{R}) \cdot \mathcal{A}_{lm}^{\mathcal{T}}(kR) d\mathbf{R} &= \frac{ik^l c}{(2l+1)!!} \sqrt{\frac{l+1}{l}} \\ &\quad \times |\langle J_f M_f | \mathcal{M}_{lm}^{\mathcal{T}} | J_i M_i \rangle|, \end{aligned} \quad (7)$$

where the nuclear transition matrix element is related to the reduced probability $B(\mathcal{T}l; J_i \rightarrow J_f)$ of nuclear transition [27]

$$B(\mathcal{T}l; J_i \rightarrow J_f) = \frac{1}{2J_i + 1} \sum_{M_i, M_f} |\langle J_f M_f | \mathcal{M}_{lm}^{\mathcal{T}} | J_i M_i \rangle|^2. \quad (8)$$

The second integral of Eq. (6), $\Xi_{fi}^{\mathcal{T}l} \equiv \int \mathbf{j}_{fi}(\mathbf{r}) \cdot \mathcal{B}_{lm}^{\mathcal{T}}(kr) d\mathbf{r}$, is associated to the electronic transition and can be deduced into the following forms

$$\Xi_{fi}^{El} \approx -\frac{eicl}{\sqrt{l(l+1)}} \int \phi_k(\mathbf{r}) \varphi_n(\mathbf{r}) h_l^{(1)}(kr) Y_{lm}(\hat{\mathbf{r}}) d\mathbf{r}, \quad (9)$$

$$\Xi_{fi}^{Ml} = 0, \quad (10)$$

where Ξ_{fi}^{El} is given to the leading order according to the condition $kr \ll 1$. Detailed derivations and discussions on $\Xi_{fi}^{\mathcal{T}l}$ are presented in the SM.

The overall transition probability per unit time is obtained explicitly as

$$\begin{aligned} P &= \frac{2\pi}{\hbar} \left(\frac{4\pi k}{c} \right)^2 \frac{k^{2l}}{[(2l+1)!!]^2} \frac{l+1}{l} \frac{B(El; J_i \rightarrow J_f) \delta(\mathcal{E}_i - \mathcal{E}_f)}{\int dE_n \rho_s(E_n)} \\ &\quad \times \sum_{n, k} F_{\mu_0, \mathcal{T}}(E_n) (1 - F_{\mu_0, \mathcal{T}}(\xi_k)) |\Xi_{fi}^{El}|^2, \end{aligned} \quad (11)$$

where $\rho_s(E)$ ($\rho_t(E)$) is the density of state at the substrate (tip). $F_{\mu_0,T}(E)$ is the Fermi–Dirac distribution of electrons in tip or substrate state with chemical potential μ_0 and temperature T . In an STM experiment, the temperature of the ultrahigh-vacuum chamber is low enough, typically lower than 10 K [46, 47], that the Fermi–Dirac distribution function is approximately a Heaviside function, i.e. $F_{\mu_0,T}(E) = 1$ for $E < \mu_0$ and $F_{\mu_0,T}(E) = 0$ for $E > \mu_0$. The transition probability per unit time is simplified as

$$P = \frac{2\pi}{\hbar} \left(\frac{4\pi k}{c} \right)^2 \frac{k^{2l}}{[(2l+1)!!]^2} \frac{l+1}{l} \frac{B(E_l; J_i \rightarrow J_f)}{\int dE_n \rho_s(E_n)} \times \int_{\mu_0 + \Delta_{eg} + eV_b}^{\mu_0} dE_n \rho_s(E_n) \rho_t(\xi_k) |\Xi_{fi}^{El}|^2, \quad (12)$$

where $\xi_k = E_n - \Delta_{eg} - eV_b$. Without loss of generality, we consider the material of the tip and the substrate to be Ag, whose density of states is obtained from Ref. [48] (see the SM for details). In the calculation, we use the reduced nuclear transition probability $B(E2; J_f \rightarrow J_i) = 27.04$ W.u. [49].

Numerical Results. — Fig. 2(a) shows the transition probability P per unit time as a function of the tip radius R_t , for fixed tip position $d = 0.5$ nm and applied bias voltage $V_b = -11$ V. The curve shows an exponential decay with the increase of the tip radius. In Eq. (12), the tip radius R_t affects the transition probability via the interaction strength Ξ_{fi}^{El} . A larger needle tip radius leads to a weaker electric field strength at the tip, yielding a lower isomeric excitation probability. And a smaller tip radius leads to a higher isomeric transition probability. For small bias voltages, a non-monotonic dependency may appear though, and the detailed discussions are presented in the SM.

Fig. 2(b) presents the dependency of the transition probability P on the tip-substrate distance d , with R_t fixed at 0.5 nm and V_b set to -11 V. The data shows that the transition probability P decreases exponentially with the increase of d . This is attributed to the decreasing overlap of wave functions between the tip and the substrate as the distance increases. A larger wave-function overlap facilitates electron tunneling between the tip and substrate, leading to an enhanced isomeric excitation probability.

Fig. 2(c) shows an approximately exponential dependency of the transition probability P on the applied bias voltage V_b , in which both d and R_t are fixed at 0.5 nm. In Eq. (12), the bias voltage V_b mainly determines the range of the energy integration. A higher V_b expands the integration range, thus allowing a broader range of energy levels to contribute to the isomeric excitation.

Discussions. — For a typical STM setup with tip radius $R_t = 0.5$ nm, tip-substrate distance $d = 0.5$ nm, and bias voltage $V_b = -11$ V, the isomeric excitation rate is calculated to be on the order of 10^{-5} s^{-1} . Here the voltage is chosen to be within the band gap of the CaF_2 crystal ($11.6 \sim 12.1$ eV) to avoid crystal damage [35]. The tip-base distance $d = 0.5$ nm is a typical parameter used in the STM experiments [50, 51] to avoid the high electron currents.

We may compare the above rate to those of existing methods. (1) The indirect optical excitation method using 29-keV

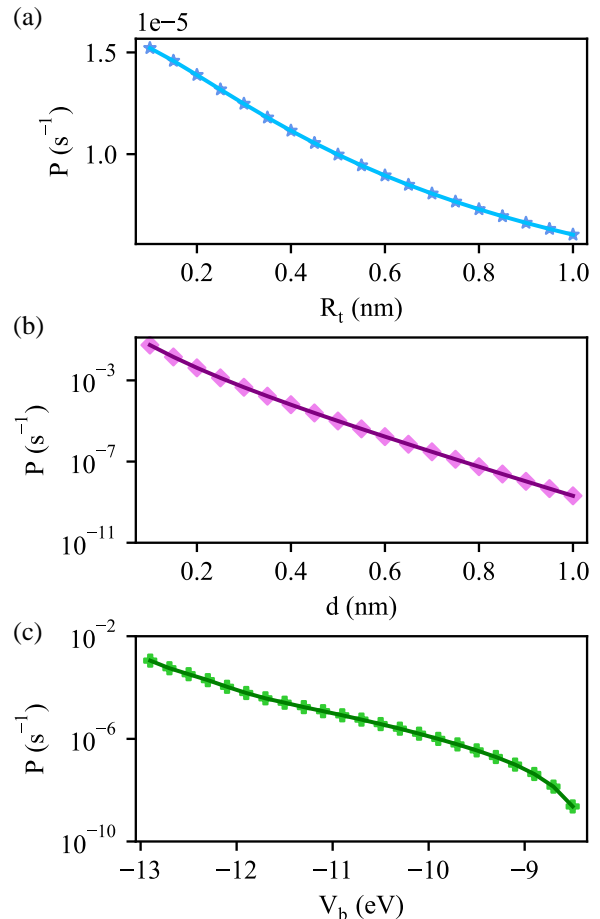


Figure 2. Transition probability per unit time P as a function of tip radius R_t , distance from the tip to the substrate d , and applied bias voltage V_b . (a) Dependency of P on R_t , with d fixed at 0.5 nm and V_b set to -11 V. (b) Dependency of P on d , with R_t fixed at 0.5 nm and V_b set to -11 V. (c) Dependency of P on V_b , with R_t fixed at 0.5 nm and d fixed at 0.5 nm. Symbols are numerical results, and curves are added to guide the eye.

synchrotron radiations yields an isomeric excitation rate on the order of 10^{-11} s^{-1} per nucleus [20]. (2) Isomeric excitation by inelastic electron scattering is most efficient for electrons around 10 eV, and the corresponding cross section is on the order of 1 mb, or 10^{-27} cm^2 [27, 28]. Assuming an electron beam with current 1 mA and beam area 1 cm^2 , the electron flux is $6.25 \times 10^{15} \text{ cm}^{-2} \text{ s}^{-1}$, and the isomeric excitation rate is about $6.25 \times 10^{-12} \text{ s}^{-1}$ per nucleus. The STM method is therefore advantageous in the excitation rate on the single-nucleus level. This is mainly due to the capability of the STM to focus the tunneling electron current on a nm-scale area.

The excitation rate has the potential to be further enhanced. Firstly, wider bandgap crystals allow higher applied bias voltages hence higher excitation rates. Secondly, trying carefully smaller tip-substrate distances (without burning out the crystal) allow higher excitation rates. These attempts are obviously challenging, but they may enhance the excitation rate

to an unprecedented high level, for example, 10^{-2} s^{-1} per nucleus. If so, together with the high photon collection efficiency of STM, active excitation and subsequent detection of nuclear radiative decay on the single-nucleus level may be realized. The quantum optical feature of nuclear γ radiation could be carefully investigated.

Conclusion.— In summary, we have proposed a new approach to use tunneling electrons in STM to excite the thorium-229 nucleus from the ground state to the low-lying isomeric state. The tunneling electrons, under an applied bias voltage, pass through the vacuum between the tip and the substrate and excite the ^{229}Th nucleus. A comprehensive theoretical framework is developed to calculate the isomeric excitation rate, and to investigate the dependency of the excitation

rate on key STM parameters, including the tip radius, the tip-substrate distance, and the applied bias voltage. The calculated single-nucleus excitation rate shows advantageous over existing methods. More importantly, our method allows nuclear excitation and control on the single-nucleus level, which is unique among all existing methods and proposals. The possibility of exciting, controlling, and detecting nuclear radiative decay on the single-nucleus level points to a completely new territory of studying nuclear physics as well as quantum optics.

This work is supported by the National Natural Science Foundation of China (NSFC) (Grants No. 12088101, No.U2230203, No. U2330401).

-
- [1] L. Kroger and C. Reich, *Nuclear Physics A* **259**, 29 (1976).
- [2] C. W. Reich and R. G. Helmer, *Phys. Rev. Lett.* **64**, 271 (1990).
- [3] B. Seiferle, L. von der Wense, P. V. Bilous, I. Amersdorffer, C. Lemell, F. Libisch, S. Stellmer, T. Schumm, C. E. Düllmann, A. Pálffy, and P. G. Thirolf, *Nature* **573**, 243 (2019).
- [4] S. Kraemer, J. Moens, M. Athanasakis-Kaklamanakis, S. Bara, K. Beeks, P. Chhetri, K. Chrysalidis, A. Claessens, T. E. Cocolios, J. a. G. M. Correia, H. D. Witte, R. Ferrer, S. Geldhof, R. Heinke, N. Hosseini, M. Huysse, U. Köster, Y. Kudryavtsev, M. Laatiaoui, R. Lica, G. Magchiels, V. Manea, C. Merckling, L. M. C. Pereira, S. Raeder, T. Schumm, S. Sels, P. G. Thirolf, S. M. Tunhuma, P. Van Den Bergh, P. Van Duppen, A. Vantomme, M. Verlinde, R. Villarreal, and U. Wahl, *Nature* **617**, 706 (2023).
- [5] E. Peik and C. Tamm, *Europhysics Letters* **61**, 181 (2003).
- [6] W. G. Rellergert, D. DeMille, R. R. Greco, M. P. Hehlen, J. R. Torgerson, and E. R. Hudson, *Phys. Rev. Lett.* **104**, 200802 (2010).
- [7] C. J. Campbell, A. G. Radnaev, A. Kuzmich, V. A. Dzuba, V. V. Flambaum, and A. Derevianko, *Phys. Rev. Lett.* **108**, 120802 (2012).
- [8] K. Beeks, T. Sikorsky, T. Schumm, J. Thielking, M. V. Okhapkin, and E. Peik, *Nature Reviews Physics* **3**, 238 (2021).
- [9] V. V. Flambaum, *Phys. Rev. Lett.* **97**, 092502 (2006).
- [10] J. C. Berengut, V. A. Dzuba, V. V. Flambaum, and S. G. Porsev, *Phys. Rev. Lett.* **102**, 210801 (2009).
- [11] G. A. Kazakov, A. N. Litvinov, V. I. Romanenko, L. P. Yatsenko, A. V. Romanenko, M. Schreitl, G. Winkler, and T. Schumm, *New Journal of Physics* **14**, 083019 (2012).
- [12] A. D. Ludlow, M. M. Boyd, J. Ye, E. Peik, and P. O. Schmidt, *Rev. Mod. Phys.* **87**, 637 (2015).
- [13] M. Safronova, *Nature* **533**, 44 (2016).
- [14] V. Barci, G. Ardisson, G. Barci-Funel, B. Weiss, O. El Samad, and R. K. Sheline, *Phys. Rev. C* **68**, 034329 (2003).
- [15] J. Thielking, M. V. Okhapkin, P. Glowacki, D. M. Meier, L. von der Wense, B. Seiferle, C. E. Düllmann, P. G. Thirolf, and E. Peik, *Nature* **556**, 321 (2018).
- [16] J. Jeet, C. Schneider, S. T. Sullivan, W. G. Rellergert, S. Mirzadeh, A. Cassanho, H. P. Jenssen, E. V. Tkalya, and E. R. Hudson, *Phys. Rev. Lett.* **114**, 253001 (2015).
- [17] A. Yamaguchi, M. Kolbe, H. Kaser, T. Reichel, A. Gottwald, and E. Peik, *New Journal of Physics* **17**, 053053 (2015).
- [18] S. Stellmer, G. Kazakov, M. Schreitl, H. Kaser, M. Kolbe, and T. Schumm, *Phys. Rev. A* **97**, 062506 (2018).
- [19] E. V. Tkalya, A. N. Zherikhin, and V. I. Zhudov, *Phys. Rev. C* **61**, 064308 (2000).
- [20] T. Masuda, A. Yoshimi, A. Fujieda, H. Fujimoto, H. Haba, H. Hara, T. Hiraki, H. Kaino, Y. Kasamatsu, S. Kitao, K. Konashi, Y. Miyamoto, K. Okai, S. Okubo, N. Sasao, M. Seto, T. Schumm, Y. Shigekawa, K. Suzuki, S. Stellmer, K. Tamasaku, S. Uetake, M. Watanabe, T. Watanabe, Y. Yasuda, A. Yamaguchi, Y. Yoda, T. Yokokita, M. Yoshimura, and K. Yoshimura, *Nature* **573**, 238 (2019).
- [21] E. V. Tkalya, *JETP Lett.* **55**, 212 (1992).
- [22] P. V. Borisyyuk, E. V. Chubunova, N. N. Kolachevsky, Y. Y. Lebedinskii, O. S. Vasiliev, and E. V. Tkalya, (2018), [arXiv:1804.00299 \[nucl-th\]](https://arxiv.org/abs/1804.00299).
- [23] S. G. Porsev, V. V. Flambaum, E. Peik, and C. Tamm, *Phys. Rev. Lett.* **105**, 182501 (2010).
- [24] B. S. Nickerson, M. Pimon, P. V. Bilous, J. Gugler, K. Beeks, T. Sikorsky, P. Mohn, T. Schumm, and A. Pálffy, *Phys. Rev. Lett.* **125**, 032501 (2020).
- [25] W. Wang, J. Zhou, B. Liu, and X. Wang, *Phys. Rev. Lett.* **127**, 052501 (2021).
- [26] J. Qi, H. Zhang, and X. Wang, *Phys. Rev. Lett.* **130**, 112501 (2023).
- [27] E. V. Tkalya, *Phys. Rev. Lett.* **124**, 242501 (2020).
- [28] H. Zhang, W. Wang, and X. Wang, *Phys. Rev. C* **106**, 044604 (2022).
- [29] E. V. Tkalya, *Chinese Physics C* **45**, 094102 (2021).
- [30] S. Gargiulo, M. F. Gu, F. Carbone, and I. Madan, *Phys. Rev. Lett.* **129**, 142501 (2022).
- [31] G. Binnig, H. Rohrer, C. Gerber, and E. Weibel, *Phys. Rev. Lett.* **49**, 57 (1982).
- [32] J. Tersoff and D. R. Hamann, *Phys. Rev. Lett.* **50**, 1998 (1983).
- [33] S.-W. Hla, *J. Vac. Sci. Technol. B* **23**, 1351 (2005).
- [34] H. Oka, O. O. Brovko, M. Corbetta, V. S. Stepanyuk, D. Sander, and J. Kirschner, *Rev. Mod. Phys.* **86**, 1127 (2014).
- [35] P. Dessoic, P. Mohn, R. A. Jackson, G. Winkler, M. Schreitl, G. Kazakov, and T. Schumm, *Journal of Physics: Condensed Matter* **26**, 105402 (2014).
- [36] D. M. Eigler and E. K. Schweizer, *Nature* **344**, 524 (1990).
- [37] P. V. Borisyyuk, O. S. Vasilyev, Y. Y. Lebedinskii, A. V. Krasavin, E. V. Tkalya, V. I. Troyan, R. F. Habibulina, E. V. Chubunova, and V. P. Yakovlev, *AIP Advances* **6**, 095304 (2016).
- [38] C. Zhang, L. Chen, R. Zhang, and Z. Dong, *Japanese Journal of Applied Physics* **54**, 08LA01 (2015).

- [39] R. Berndt, R. Schlittler, and J. Gimzewski, *Journal of Vacuum Science & Technology B: Microelectronics and Nanometer Structures Processing, Measurement, and Phenomena* **9**, 573 (1991).
- [40] G. Dong, Y. You, and H. Dong, *New Journal of Physics* **22**, 113010 (2020).
- [41] G. Dong, Z. Hu, X. Sun, and H. Dong, *J. Phys. Chem. Lett.* **12**, 10034 (2021).
- [42] J. Bardeen, *Phys. Rev. Lett.* **6**, 57 (1961).
- [43] A. D. Gottlieb and L. Wesoloski, *Nanotechnology* **17**, R57 (2006).
- [44] C. J. Chen, *Phys. Rev. B* **42**, 8841 (1990).
- [45] J. M. Eisenberg and W. Greiner, *Nuclear Theory. Excitation mechanisms of the nucleus. Vol. 2* (North-Holland Publishing Company, Amsterdam-London, 1976).
- [46] G. Binnig and H. Rohrer, *Rev. Mod. Phys.* **59**, 615 (1987).
- [47] P. K. Hansma, V. B. Elings, O. Marti, and C. E. Bracker, *Science* **242**, 209 (1988).
- [48] Z. Lin, L. V. Zhigilei, and V. Celli, *Phys. Rev. B* **77**, 075133 (2008).
- [49] N. Minkov and A. Pálffy, *Phys. Rev. Lett.* **118**, 212501 (2017).
- [50] J. A. Stroschio and D. M. Eigler, *Science* **254**, 1319 (1991).
- [51] J. Kröger, A. Sperl, N. Néel, and R. Berndt, *Journal of Scanning Probe Microscopy* **4**, 49 (2009).